Available online at www.sciencedirect.com
SCIENCE DIRECT®
Journal of Solid State Chemistry 179 (2006) 590–596
JOURNAL OF SOLID STATE CHEMISTRY
www.elsevier.com/locate/jssc

Nanosized $LiMn_2O_4$ from mechanically activated solid-state synthesis

V. Massarotti*, D. Capsoni, M. Bini

Dipartimento di Chimica Fisica "M. Rolla" e IENI-CNR, viale Taramelli 16, 27100 Pavia, Italy

Received 21 July 2005; received in revised form 18 November 2005; accepted 20 November 2005
Available online 27 December 2005

Abstract

The synthesis of pure and Cr-doped nanosized $LiMn_2O_4$ particles has been carried out by solid-state process on high-energy ground mixtures. In situ X-ray analysis demonstrates the spinel forms as single phase at 623 K passing through the Mn_3O_4 precursor at temperatures as low as 573 K. In the doped high-energy ground mixture Li-rich spinel phase forms at 623 K and Cr ions insert in the spinel octahedral site only at 723 K.

A mean particle size value of 60 Å, quite independent of the reaction time, is obtained for $T<673$ K. For higher temperature the growing of the particles as a function of time is observed, independent of doping. The mechanical grinding seems to be the most suitable way to obtain impurity-free spinel phases at lower temperature and with smaller particle size with respect to manually ground mixtures by solid-state reaction and via sol–gel synthesis.

Keywords: Nanostructures; X-ray powder diffraction; Scanning electron microscopy; Crystallite size.

1. Introduction

$LiMn_2O_4$ is an appealing cathode material for lithium batteries [1–4], due to its room temperature (RT) conductivity, related to electron hopping contribution [5,6] and also to possible mobile Li^+ ions intercalation/de-intercalation in the cationic framework [1,3].

The cubic spinel-type structure, stable for $T>285$ K, for lower temperature undergoes an orthorhombic transition [7,8], induced by the Jahn–Teller (JT) distortion of Mn^{3+} ions sites. The transition, depending on Mn^{3+} concentration, can be inhibited by reducing the Mn^{3+} amount. Recent studies showed that the inhibition of the JT distortion can be reached both by suitable cationic substitution on Mn site [9–13], such as Cr^{3+} ions, and by stoichiometry deviations induced by Li excess with respect to 0.333 cationic fraction [14–17].

$LiMn_2O_4$ easily forms by conventional solid-state reaction, but lot of work was devoted to their preparation by other routes, with the aim to obtain both impurity-free and small particle size samples [18–24]. A sol–gel route [25] leads to the formation of small crystallite size by annealing at temperatures lower than for solid-state processes. However, for $T\leqslant 973$ K the spinel is not a single phase and traces of Mn oxides disappear at 1073 K [26].

The aim of the present study is to synthesize pure and Cr-doped $LiMn_2O_4$ nanoparticles at temperatures as low as possible and to study the reaction mechanism by in situ X-ray powder diffraction (XRPD). Mixtures of the reagents prepared by different degree of mixing (manual grinding (G) or mechanical grinding (MG)) are studied in situ at different temperatures. Starting from Cr_2O_3-doped reacting mixtures, also the Cr substitution on Mn site can be studied. Both crystallite sizes and phase abundance were evaluated by analysing shapes, breadth and integrated intensity of the Bragg peaks. Moreover, the product stoichiometry is discussed on the ground of the lattice parameters values, taking into account the influence of both lithium stoichiometry deviations and dopant substitution on the Mn site. The relations among temperature, phase composition and crystallite size of the spinel are discussed.

*Corresponding author. Fax: +39 382 987575.
E-mail address: vincenzo.massarotti@unipv.it (V. Massarotti).

0022-4596/$ - see front matter © 2005 Elsevier Inc. All rights reserved.
doi:10.1016/j.jssc.2005.11.019

2. Experimental

$LiMn_2O_4$ spinel was obtained by mixing MnO and Li_2CO_3 in stoichiometric amount. Doped samples were prepared by substituting to MnO the proper amount of Cr_2O_3 to reach the 5% of Cr substitution on Mn site. Each sample was manually ground in an agate mortar and mechanically ground by high-energy ball milling. Samples of about 10 g were milled for 2 and 5 h in a high-energy, high-capacity vibratory ball mill in air atmosphere. The grinding balls (carbon steel) to powder ratio was 20:1. Other details were reported elsewhere [27]. The formation reaction of pure and doped $LiMn_2O_4$ was directly monitored by in-situ XRPD at different temperatures and, at the same temperature, as a function of time on the G and 5 h MG mixtures.

XRPD measurements were performed with a Bruker D5005 diffractometer provided with a scintillation detector and a curved graphite monochromator on the diffracted beam; Cu$K\alpha$ radiation was used. For high-temperature (HT) XRPD measurements an HTK1200, Anton Paar polythermal attachment was used. Quick response was obtained by means of a position sensitive detector. The patterns were collected in the temperature range 298–1073 K, depending on sample. For time-dependent measurements, the reaction evolution was followed within 17 h.

Scanning electron microscopy (SEM) micrographs were collected by a Cambridge Stereoscan 200 SEM on gold sputtered samples.

3. Results

The effect induced by MG on the starting mixture has been studied by both XRPD and SEM analysis. In Fig. 1, the diffraction patterns of undoped G and 2 and 5 h MG mixtures are compared. As expected, only the MnO and Li_2CO_3 diffraction peaks are observed in the G sample: the peaks height and broadening decreases and increases, respectively, with increasing the grinding time. These effects are more evident for the reflections pertinent to the Li_2CO_3 phase. In addition, the MG induces some oxidation of MnO to Mn_3O_4 as demonstrated by the presence of very broadened peaks at about 32.3° and 36°, more evident in the 5 h MG mixture. The application of the Scherrer equation was carried out for the MG mixtures on the full-width at half-maximum (FWHM) for (200) MnO and (−110) Li_2CO_3 diffraction reflections; the use of FWHM instead of the integral breath is justified by the large broadening of peaks. The results of the crystallite size are reported in Table 1 and compared with the very large values, not valuable on the basis of the Scherrer equation, of MnO and Li_2CO_3 before grinding. In the Cr 5% doped starting mixtures, the Cr_2O_3 component is observed together with MnO and Li_2CO_3 (see inset in Fig. 1); the MG affects peak intensity and broadening as already evidenced for the undoped sample.

SEM micrographs are obtained on reagents and both doped and pure mixtures after G and MG. Fig. 2 shows the micrographs of the MnO and Li_2CO_3 reagents (Fig. 2a and 2b respectively); as an example, the micrographs after G and 5 h MG of the undoped mixture are shown (Fig. 2c and

Table 1
Crystallite size dimensions of reagents before and after mechanical grinding for different time

	G	2 h MG	5 h MG
MnO (Å)	>3000	360	260
Li_2CO_3 (Å)	>3000	100	<100

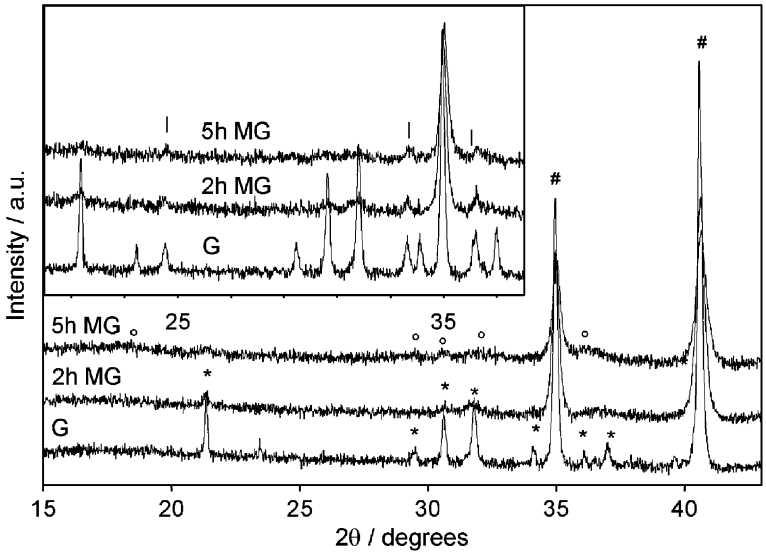

Fig. 1. XRPD patterns of undoped and doped (inset) starting mixtures after different grinding. (#) MnO, (*) Li_2CO_3, (°) Mn_3O_4 and (|) Cr_2O_3 main peaks.

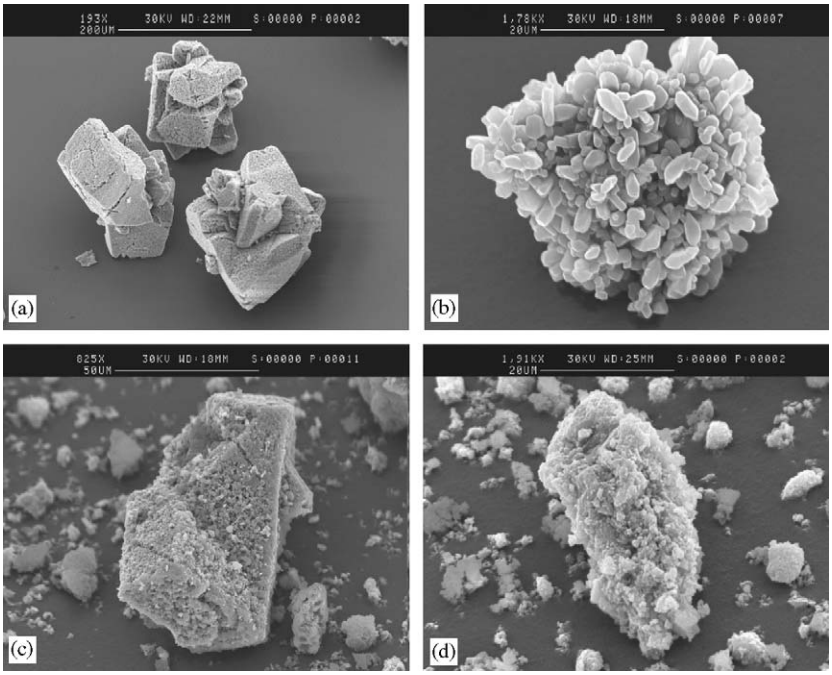

Fig. 2. SEM micrographs of (a) MnO, (b) Li_2CO_3, (c) undoped G mixture and (d) undoped 5 h MG mixture.

2d respectively). MnO surfaces highly covered by Li_2CO_3 small particles are obtained after MG (Fig. 2d).

The HT XRPD measurements on the 5 h MG undoped mixture in the 473–623 K temperature range are reported at the beginning (Fig. 3a) and at the end (Fig. 3b) of the isothermal process, when no further reaction progress is observed. The $LiMn_2O_4$ phase forms in small amount already at 473 K while MnO and Li_2CO_3 decrease and Mn_3O_4 abundance increases with respect to the starting mixture (see for comparison Fig. 1 and Fig. 3a). Phase amount does not appreciably change after time as high as 15 h at 473 K (Fig. 3b). The same crystallographic phases are observed at 523 K, where traces of Mn_5O_8 are also present: no evolution of the reacting system is observed after 13 h at this temperature. With increasing temperature the $LiMn_2O_4$ amount increases; after 5 h at 573 K traces of MnO and Mn_3O_4 are still observed, while at 623 K the lithium manganese spinel is the only phase present.

XRPD measurements before and after annealing at different temperature ($523 < T < 723$ K) on 5 h MG Cr 5% doped mixture show very similar results with respect to the pure samples (Fig. 3), as it is shown in Fig. 4a and b. After 6 h at 673 K, the reaction progress is similar to that of 623 K; at 723 K Cr_2O_3 peaks disappear and only doped $LiMn_2O_4$ is obtained within 10 h.

The patterns of the G mixture for the undoped sample collected at the beginning of the annealing for $673 \leqslant T \leqslant 973$ K are reported in Fig. 5. The Li_2CO_3 is present up to 773 K. It was verified that some Li_2CO_3 peaks whose position is particularly dependent on c-axis, e.g., the (−202) and (002) found at 29.77° and 31.32°, respectively, for $T = 773$ K, are significantly shifted towards lower angle with respect to the literature RT data (30.61° and 31.80°). Instead, the (−110) reflection, not dependent on c, shows a 2θ position at 773 K very close to the RT value. This effect can be explained on the basis of a strong thermal expansion along the c-axis and/or distortion in β monoclinic angle with increasing temperature. As expected, the MnO amount decreases up to 873 K, while $LiMn_2O_4$ phase increases and coexists, for $T \geqslant 773$ K, with Li_2MnO_3, whose amount decreases with T. The Mn_3O_4 intermediate phase is present only for $773 \leqslant T \leqslant 873$ K. Comparable results are obtained from HT measurements on the G Cr 5% doped mixture. Cr_2O_3 is observed up to 773 K and coexists with Li_2CrO_4 at 673 K (see inset of Fig. 5).

Fig. 6 shows the crystallite size as a function of time at different temperature for the 5 h MG-doped sample. Similar trends are observed for the 5 h MG undoped mixture. As an example the 573 K data are reported, while other isotherms data are omitted for sake of simplicity.

Fig. 7 shows lattice parameters a (a) and crystallite size $\langle D \rangle$ (b) as a function of temperature for G and MG samples. The a and $\langle D \rangle$ values are compared with data from $LiMn_2O_4$ thermal expansion [28] and sol–gel synthesis [26], respectively.

4. Discussion and conclusions

The influence of the grinding on the reactivity of the samples can be deduced by comparing the results shown in Fig. 1 and Table 1. The MG process strongly reduces the crystallite size from about 3000 Å to about 260 and 100 Å for MnO and Li_2CO_3, respectively. Simultaneously to the large decrease of the MnO particle size after 5 h MG, the

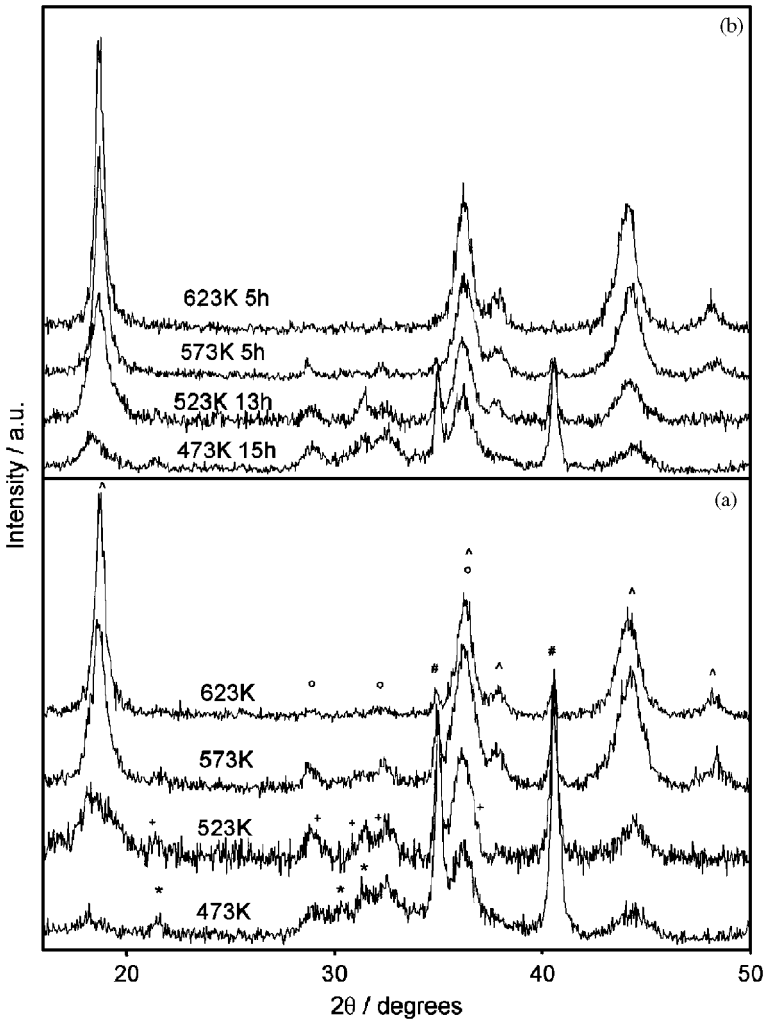

Fig. 3. XRPD patterns of 5 h MG undoped mixture at different temperatures (a) at the beginning and (b) at the end of the isothermal process. (#) MnO, (^) $LiMn_2O_4$, (°) Mn_3O_4, (*) Li_2CO_3 and (+) Mn_5O_8 main peaks.

formation of small amounts of Mn_3O_4 phase is observed (Fig. 1). The same oxidation effect was previously reported on mechanical activated MnO–Li_2CO_3 mixture [24]. This evidence can be due to oxidation process of the MnO grain boundary just formed in air under the possible local heating induced by the high-energy grinding.

The SEM micrographs put into evidence both the mixing degree of the reagents and the particle morphology and size, very important features for the reactivity of the mixture. Before grinding, large agglomerates (about 100–200 μm) are observed for MnO particles (Fig. 2a) while rather fine ones (about 20 μm) are present in Li_2CO_3 (Fig. 2b). The G of the mixture slightly reduces the oxide particles size (about 50–80 μm, Fig. 2c) but a non-homogeneous layer of fine Li_2CO_3 covers MnO. The strong difference in the particle size of the two reagents leads to a mixing but not to a significant reduction of the agglomerates size. A high mixing degree and small particle size are obtained after 5 h MG (Fig. 2d). The microsized MnO phase (5–15 μm) is uniformly covered by Li_2CO_3 component, even if some differences in the MnO and Li_2CO_3 agglomerate sizes are justified by the different hardness degree between the phases. The XRPD measurements at 473 K for the undoped MG mixture (Fig. 3) put into evidence the increase of the Mn_3O_4 amount, possibly due to the previous formation of this phase at RT (Fig. 1). $LiMn_2O_4$, obtained at 473 K in small amount, is completely formed after 5 h at 623 K (Fig. 3b). This demonstrates the efficiency of the solid-state synthesis via high-energy grinding with respect to the sol–gel route, where much higher temperatures are necessary to obtain single phase spinel [26]. For what concerns the MG-doped mixture, the spinel phase is nearly completely formed after 10 h at 623 K (Fig. 4b), in agreement with the undoped case. However, a significant amount of Cr_2O_3 is still observed and only after 10 h at 723 K it completely inserts into the spinel phase. In other words, for $T \leqslant 723$ K Cr_2O_3 phase does not completely participate in the spinel formation and a non-stoichiometric Li-rich spinel must be considered. For such phase, we should consider a charge distribution on the

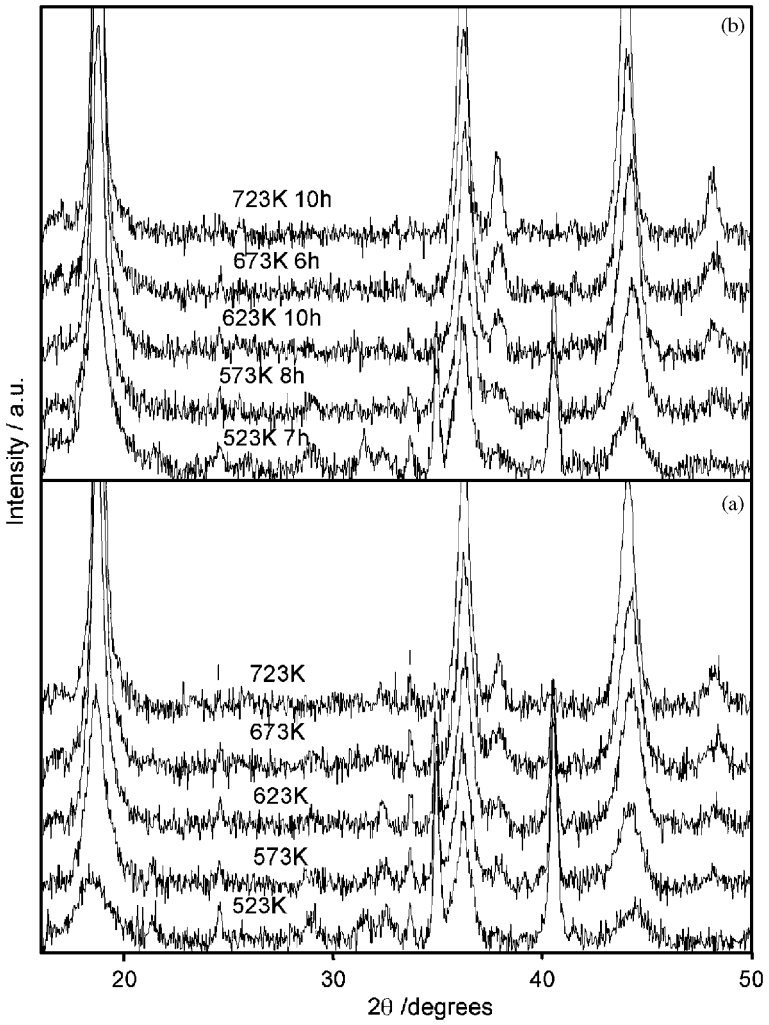

Fig. 4. XRPD patterns of 5 h MG-doped mixture at different temperatures (a) at the beginning and (b) at the end of the isothermal process. (|) Cr_2O_3 main peaks. The symbols pertinent to the other phases, corresponding to those observed in Fig. 3, are omitted for sake of simplicity.

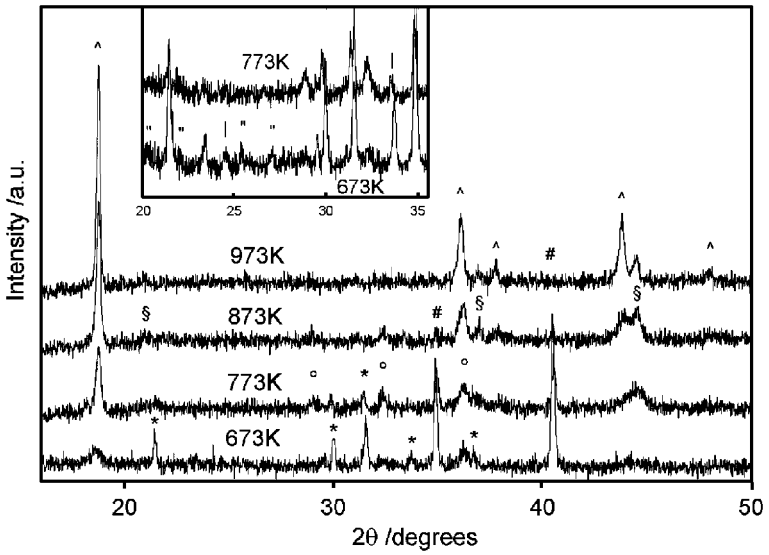

Fig. 5. XRPD patterns at different temperatures of undoped G mixture. The inset shows two selected temperatures for doped G mixture. (^) $LiMn_2O_4$, (§) Li_2MnO_3, (#) MnO, (*) Li_2CO_3, (°) Mn_3O_4, (|) Cr_2O_3 and (″) Li_2CrO_4 main peaks.

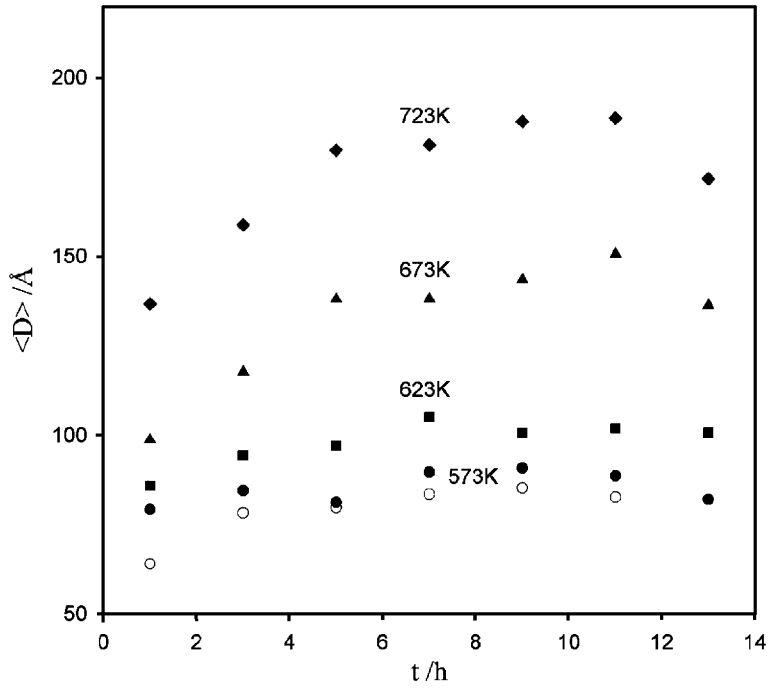

Fig. 6. Crystallite size as a function of time for the undoped (open symbol) and doped (full symbol) 5 h MG mixtures at different temperatures.

octahedral frame represented by [10]

$$[Li_y^+ Cr_x^{3+} Mn_{1-3y-x}^{3+} Mn_{1+2y}^{4+}] \quad \text{with } 0 \leqslant x \leqslant 0.10.$$

Taking into account an initial molar ratio Li/Mn = 1/1.90 ($x = 0.10$ for the 5% doped sample), a value $y = 0.034$ is obtained when $x = 0$, i.e., for $T < 623$ K, when the Cr^{3+} dissolution is not yet begun. At $T \geqslant 723$ K, after the complete insertion of Cr^{3+} in the spinel phase, $x = 0.10$ and $y = 0.00$. The presence of the Li-rich spinel at 623 K for the doped mixture agrees with the lower lattice parameter value with respect to the undoped sample, where the spinel seems to be more stoichiometric, as demonstrated by the a value closer to that evaluated by thermal expansion at the same temperature (Fig. 7a). By comparing the XRPD reactivity results of the doped mixture at different temperature and the crystallite size of the spinel phase (Fig. 6) it can be deduced that the Cr substitution on Mn site is obtained during the growing of $LiMn_2O_4$ particles. In particular, for $T \leqslant 623$ K a constant size value independent of time is obtained, while, for higher temperatures, the particle size grows with time for each isothermal process (Fig. 6) and Cr_2O_3 disappears.

The comparison between the XRPD results of G and MG undoped mixture (Fig. 5 and Fig. 3a) shows that, in the former case, the reaction starts at a temperature at least 200 K greater: Li_2CO_3 is observed up to 673 K, MnO phase disappears at 873 K (Fig. 5) and Mn_3O_4 is stable up to 873 K. Moreover, Li_2MnO_3 forms at $773 \leqslant T \leqslant 873$ K together with spinel and Mn_3O_4 phases. Similar results are obtained from the G-doped mixture. G and MG mixtures differ for what concerns the Cr–Mn insertion mechanism: in the G case, Cr_2O_3 reacts partially at 673 K forming Li_2CrO_4 (inset of Fig. 5). At 773 K the Cr oxide phases are not detected, so the Cr insertion in $LiMn_2O_4$ spinel passes through the formation of Li_2CrO_4. Moreover, the doping step happens during the early $LiMn_2O_4$ lattice formation when other phases coexist (inset of Fig. 5), while for the MG case (Fig. 4) the Cr ions substitute during the growth of the Li-rich spinel phase (Fig. 6).

The mechanism of formation of undoped and Cr-doped $LiMn_2O_4$ can be summarized by comparing the lattice parameters (Fig. 7a) and crystallite size (Fig. 7b) as a function of temperature. The a values obtained from the thermal expansion study of $LiMn_2O_4$ previously synthesized (Fig. 7a) [28] are higher than those obtained when the spinel is under formation and coexists with other phases, independent of the grinding and doping. Only for $T \geqslant 973$ K, when the spinel phase is the main component, the a parameter reaches the same value independent of the synthesis route. For $T < 973$ K, the MG samples lead to higher a values with respect to the G ones. In this last case, the spinel coexists with other impurity phases in a larger temperature range and hence stoichiometry deviations, influencing the a parameter, may be expected [5]. Indeed, the lattice parameter value of the pure MG sample, after cooling down to RT (Fig. 7a), is in a very good agreement with that reported for $LiMn_2O_4$ (8.2426 Å). This result confirms that the desired stoichiometry in $LiMn_2O_4$ is obtained.

The microstructural analysis (Fig. 7b) shows a very similar growing of crystallite size as a function of temperature for both undoped and doped MG samples. The size trend is shifted at higher temperatures for the G

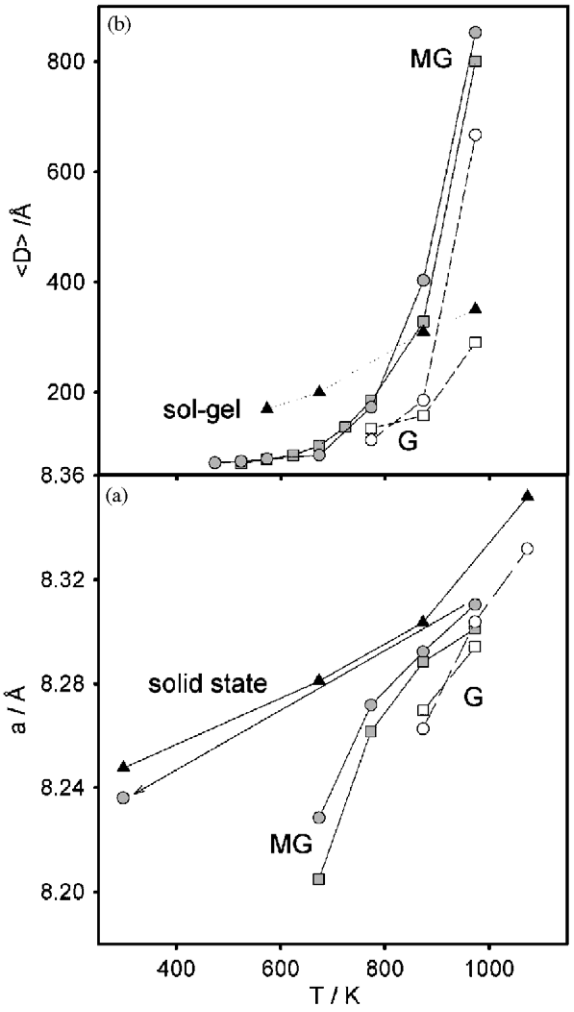

Fig. 7. Temperature dependence of (a) lattice parameters and (b) crystallite size of undoped (circle) and doped (square). Open, grey and black symbols refer to G, MG and literature [26,28] data, respectively. Standard deviations are comparable to the symbol size.

samples and higher values are obtained for pure sample with respect to the doped one at 973 K, so suggesting a doping effect on the $\langle D \rangle$ values. A comparison with the crystallite size obtained by sol–gel synthesis of the spinel phase [26] shows that the $\langle D \rangle$ slightly depends on temperature but higher values are obtained for $T < 823$ K.

In conclusion, the MG synthesis shows some advantage with respect to the sol–gel route: a stoichiometric and impurity-free spinel phase is obtained at 623 K for undoped sample and at 723 K for the doped one, in a temperature range much lower than that necessary for the undoped sol–gel samples ($T > 973$ K) [26]. Moreover, nanosized lithium manganese spinel particles are obtained, thanks to the lower temperature synthesis.

Acknowledgments

The valuable help of Dr. R. Ricceri in performing the high-energy grinding of the mixtures is gratefully acknowledged.

References

[1] J.M. Tarascon, D. Guyomard, Electrochim. Acta 38 (1993) 1221–1231.
[2] H. Berg, O. Bergstrom, T. Gustaffson, E. Kelder, J.O. Thomas, J. Power Sour. 68 (1997) 24–29.
[3] P.G. Bruce, Philos. Trans. R. Soc. Lond. Ser. A 354 (1996) 1577–1594.
[4] B. Ammundsen, G.R. Burns, M. Saiful Islam, H. Kanoh, J. Roziere, J. Phys. Chem. B 103 (1999) 5175–5180.
[5] V. Massarotti, D. Capsoni, M. Bini, G. Chiodelli, C.B. Azzoni, M.C. Mozzati, A. Paleari, J. Solid State Chem. 131 (1997) 94–100.
[6] E. Iguchi, N. Nakamura, A. Aoki, Philos. Mag. B 78 (1998) 65–77.
[7] J. Rodriguez-Carvajal, G. Rousse, C. Masquelier, M. Hervieu, Phys. Rev. Lett. 81 (1998) 4660–4663.
[8] V. Massarotti, D. Capsoni, M. Bini, P. Scardi, M. Leoni, V. Baron, H. Berg, J. Appl. Crystallogr. 32 (1999) 1186–1190.
[9] D. Capsoni, M. Bini, G. Chiodelli, V. Massarotti, M.C. Mozzati, C.B. Azzoni, Solid State Commun. 125 (2003) 179–183.
[10] D. Capsoni, M. Bini, G. Chiodelli, V. Massarotti, C.B. Azzoni, M.C. Mozzati, A. Comin, Phys. Chem. Chem. Phys. 3 (2001) 2162–2166.
[11] D. Capsoni, M. Bini, G. Chiodelli, V. Massarotti, P. Mustarelli, L. Linati, M.C. Mozzati, C.B. Azzoni, Solid State Commun. 126 (2003) 169–174.
[12] C. Bellitto, M.C. DiMarco, V.R. Branford, M.A. Green, D.A. Neumann, Solid State Ionics 140 (2001) 77–81.
[13] S. Suzuki, M. Tomita, S. Okada, H. Arai, J. Phys. Chem. Solids 57 (1996) 1851–1856.
[14] C.B. Azzoni, M.C. Mozzati, A. Paleari, M. Bini, D. Capsoni, G. Chiodelli, V. Massarotti, Z. Naturforsch. 54a (1999) 579–584.
[15] C.B. Azzoni, M.C. Mozzati, A. Paleari, V. Massarotti, M. Bini, D. Capsoni, Z. Naturforsch. 53a (1998) 771–778.
[16] V.W.J. Verhoeven, F.M. Mulder, I.M. deSchepper, Physica B 276–278 (2000) 950–951.
[17] I. Shiraishi, I. Nakai, T. Tsubata, T. Himeda, F. Nishikawa, J. Power Sour. 81–82 (1999) 571–574.
[18] C. Chu, B. Dunn, J. Am. Ceram. Soc. 70 (1987) C375–C377.
[19] W. Liu, G.C. Farrington, F. Chaput, B. Dunn, J. Electrochem. Soc. 143 (1996) 879–884.
[20] S.R.S. Prabaharan, N.B. Saparil, S.S. Michael, M. Massot, C. Julien, Solid State Ionics 112 (1998) 25–34.
[21] Y.S. Lee, Y.K. Sun, K.S. Nahm, Solid State Ionics 109 (1998) 285–294.
[22] N. Kosova, E. Devyatkina, Solid State Ionics 172 (2004) 181–184.
[23] N.V. Kosova, E.T. Devyatkina, S.G. Kozlova, J. Power Sour. 97–98 (2001) 406–411.
[24] N.V. Kosova, N.F. Uvarov, E.T. Devyatkina, E.G. Avvakumov, Solid State Ionics 135 (2000) 107–114.
[25] P. Barboux, J.M. Tarascon, F.K. Shokoohi, J. Solid State Chem. 94 (1991) 185–196.
[26] V. Massarotti, D. Capsoni, M. Bini, G. Chiodelli, C.B. Azzoni, M.C. Mozzati, A. Paleari, J. Solid State Chem. 147 (1999) 509–515.
[27] D. Basset, P. Matteazzi, F. Miani, Mater. Sci. Eng. A 168 (1993) 149–152.
[28] V. Massarotti, D. Capsoni, M. Bini, Solid State Commun. 122 (2002) 317–322.